

Motility-Induced Pinning in Flocking System with Discrete Symmetry

Chul-Ung Woo and Jae Dong Noh

Department of Physics, University of Seoul, Seoul 02504, Korea

(Dated: September 30, 2024)

We report a motility-induced pinning transition in the active Ising model for a self-propelled particle system with discrete symmetry. This model was known to exhibit a liquid-gas type flocking phase transition, but a recent study reveals that the polar order is metastable due to droplet excitation. Using extensive Monte Carlo simulations, we demonstrate that, for an intermediate alignment interaction strength, the steady state is characterized by traveling local domains, which renders the polar order short-ranged in both space and time. We further demonstrate that interfaces between colliding domains become pinned as the alignment interaction strength increases. A resonating back-and-forth motion of individual self-propelled particles across interfaces is identified as a mechanism for the pinning. We present a numerical phase diagram for the motility-induced pinning transition, and an approximate analytic theory for the growth and shrink dynamics of pinned interfaces. Our results show that pinned interfaces grow to a macroscopic size preventing the polar order in the regime where the particle diffusion rate is sufficiently smaller than the self-propulsion rate. The growth behavior in the opposite regime and its implications on the polar order remain unresolved and require further investigation.

Introduction – Active matter, consisting of self-propelled particles (SPPs), displays intriguing collective phenomena [1, 2]. SPPs, such as migrating cellular organisms [3–5], swarming animals [6–11], synthetic materials [12–15], and so on, convert internal or external energy into kinetic motion. The self-propulsion distinguishes active matter from thermal equilibrium systems. When SPPs interact through local velocity alignment, they can exhibit long-range polar order with broken continuous symmetry, even in two dimensions [16, 17]. This is in contrast to thermal equilibrium systems, where the Mermin-Wagner theorem prohibits such ordering [18]. Repulsive interactions among SPPs can lead to a phase separation, whereas attractive interactions would be necessary in thermal equilibrium systems [19–22]. Active matter systems incorporating other elements, such as discrete symmetry [23–30], multiple species [31–33], and quenched disorder [34–37], have been attracting growing interest.

The Vicsek model is a well-established model for the flocking transition [16]. It comprises SPPs whose self-propulsion direction is represented by a continuous XY spin variable. Both a field-theoretic renormalization group study [17, 38] and extensive numerical simulations confirm that the model indeed exhibits the long-range polar order [39–45]. The active Ising model (AIM) is a discrete version of the Vicsek model [24, 25]. As a discrete model, it enables large scale numerical simulations and facilitates an analytically tractable hydrodynamic theory [40, 46, 47]. The system has been known to exhibit a liquid-gas type phase transition between a disordered (gas) phase and a polar ordered (liquid) phase. These phases are separated by a coexistence phase where particles are phase separated into gas and liquid regions. The liquid region forms a macroscopic band traveling over the gaseous background. The liquid-gas transition picture has also been confirmed in the Vicsek model with a modification that macrophase separation is replaced

with microphase separation in the coexistence phase [48].

Recent studies have revealed the fragility of the long-range polar order in active matter systems. In the Vicsek model, a single point-like obstacle or a finite counter-propagating blob can disrupt the global polar order [49]. The AIM exhibits even greater fragility [50]. When the system is prepared in an ordered state, droplets spontaneously nucleate and counter-propagate at a constant speed, ultimately destroying the initial polar order. These findings raise an interesting question: does the long-range polar order truly exist in the active matter systems with discrete symmetry? If not, what would be the asymptotic phase?

This Letter addresses those questions specifically in the context of the AIM. We demonstrate numerically that both the ordered and the coexisting states in the liquid-gas transition scenario ultimately evolve to a state consisting of randomly oriented finite-size traveling droplets, rendering the polar order short-ranged in both space and time. Interestingly, we discover as the alignment interaction strength increases further, the system undergoes a *motility-induced pinning* (MIP) transition instead of the expected liquid-gas transition. In the pinned phase, interfaces between domains oriented in opposite directions become immobile. Individual particles accumulate near these interfaces and exhibit a back and forth resonating motion. We will provide a numerical evidence for the MIP and its analytic justification, and discuss the implication of the MIP on the polar order in the last section.

Active Ising model – The AIM [24] comprises N SPPs on a two-dimensional (2D) lattice of $L_x \times L_y$ sites with periodic boundary conditions. The overall density is denoted as $\rho_0 = N/(L_x L_y)$. Each particle is associated with an Ising spin variable, $s = \pm 1$, indicating its self-propulsion direction. Particles hop to one of their four neighbors at diffusion rate $4D$, self-propel to a neighboring site on the right ($s = +1$) or left ($s = -1$) at rate v , and can flip

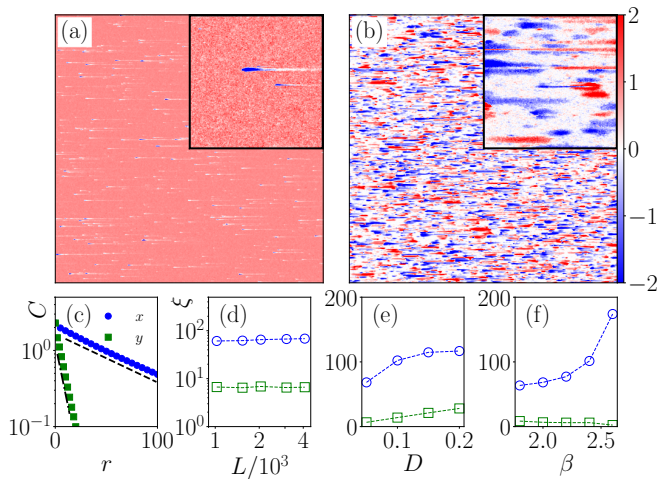


FIG. 1. Snapshots taken at 4×10^3 MCS in (a) and 5×10^4 MCS in (b) of an initially ordered system of size 4096^2 . The insets present an enlarged view of a subsystem of size 256^2 . The normalized magnetization m/ρ_0 is color-coded according to the color bar. (c) Magnetization correlation functions in the steady state along the x and y directions (symbols) following an exponential decay (dashed lines). [Parameters: $L = L_x = L_y = 4096$, $\rho_0 = 8$, $D = 0.05$, $v = 1$, and $\beta = 2$] Also shown is the dependence of ξ_x (circles) and ξ_y (squares) on L in (d), D in (e), and β in (f).

their spin state ($s \rightarrow -s$) at rate $w e^{-\beta s m_{\mathbf{r}}/\rho_{\mathbf{r}}}$, where $\rho_{\mathbf{r}}$ and $m_{\mathbf{r}}$ denote the number of particles and the magnetization at the residing site $\mathbf{r} = (x, y)$, respectively. The ratio $p_{\mathbf{r}} = m_{\mathbf{r}}/\rho_{\mathbf{r}}$ is called the polarization. We will set $w = 1$. The parameter β , called the inverse temperature, represents a strength of an alignment interaction of self-propulsion directions. The polar order manifests itself as a ferromagnetic order.

The AIM can be described by the continuum hydrodynamic equation, based on a local mean-field approximation, for the density field $\rho = \rho(\mathbf{r}, t)$ and the magnetization field $m = m(\mathbf{r}, t)$ [25, 46, 47, 50]:

$$\begin{aligned} \partial_t \rho &= \nabla \cdot D \nabla \rho - v \partial_x m \\ \partial_t m &= \nabla \cdot D \nabla m - v \partial_x \rho + F(\rho, m) \end{aligned} \quad (1)$$

Here, $F(\rho, m) = 2\rho \sinh(\beta m/\rho) - 2m \cosh(\beta m/\rho)$, and the diffusion matrix D is diagonal with elements $D_x = D + v/2$ and $D_y = D$.

We have simulated the AIM dynamics using a parallel update Monte Carlo (MC) method. During one MC sweep (MCS), corresponding to a time interval $\Delta t = 1/(4D + v + e^\beta)$, all particles attempt hopping, self-propulsion, or spin flip in parallel [51].

Metastability of ordered and coexistence phases – We confirm the metastability of the ordered state (see Fig. 1), which was first reported in Ref. [50]. The system, starting from an ordered initial state, evolves into a state with multiple traveling droplets, nucleated spontaneously. These droplets grow and merge into larger ones.

At the same time, they also suffer from spontaneous nucleation of droplets of opposite polarization, and break up into smaller pieces. This competition between growth and break-up drives the system to a steady state with randomly distributed local domains [52].

The characteristic size of droplets is estimated using the correlation function $C(\mathbf{r}) := \sum_{\mathbf{r}_0} \langle m_{\mathbf{r}+\mathbf{r}_0} m_{\mathbf{r}_0} \rangle_{ss} / (\rho_0^2 L_x L_y)$, where $\langle \rangle_{ss}$ denotes a steady state time average. As shown in Fig. 1(c), it decays exponentially with distance in both x and y directions. Importantly, the characteristic sizes ξ_x and ξ_y converge to finite values as the system size increases (Fig. 1(d)). The characteristic sizes vary smoothly with other parameters like D and β (Fig. 1(e, f)). These observations collectively indicate that the polar order in the steady state is short-ranged in both space and time.

The coexistence phase is also found to be metastable [52]. A droplet nucleates spontaneously inside a band and grows to a size $\xi = O(L_x)$ before escaping into the disordered background. Continuing its ballistic movement, it evaporates as constituent particles diffuse away. Notably, this diffusive evaporation would take a time $\tau_{\text{evap}} \propto \xi^2$, while collision with the band takes $\tau_{\text{col}} \propto L_x$. Therefore, in sufficiently large systems, the droplet repeatedly invades the band, ultimately destroying it. In the infinite system, a liquid band itself is macroscopic, hence metastable as the liquid state is.

Motility-induced pinning – Numerical results suggest that the AIM exhibits only a crossover to a locally ordered state, not a sharp liquid-gas transition. The global polar order is hindered by the droplet excitation [50]. We will demonstrate, however, that these traveling droplets cease to exist as the inverse temperature β increases further, and the system undergoes a MIP transition. As β increases, two distinct time scales emerge: one for spin flips (fast process with rate $\sim e^\beta$) and the other for particle motion (slow process with rate $4D + v$). This separation of time scales significantly impacts droplet dynamics.

Consider the limiting case $\beta \rightarrow \infty$. When a particle moves to a nonempty site, the particle's spin instantly aligns with the polarization at the target site. Consider two local domains of opposite polarization confronting each other with a domain wall or an interface separating them. Particles near the interface exhibit a back-and-forth oscillation: whenever a particle self-propels across the interface, it flips its self-propulsion direction and returns, and this process repeats. Consequently, the interface will be pinned in space. In analogy to the resonance structures found in chemical bonds [53], this oscillating motion will be called resonance. When $v = 0$ (without self-propulsion), the resonance disappears, and the interfaces are never pinned. In 1D, a pinned interface becomes a point defect [54].

The MIP phenomenon persists for finite values of β , as demonstrated in Fig. 2. The pinning is characterized by f_p , the fraction of particles trapped in pinned inter-

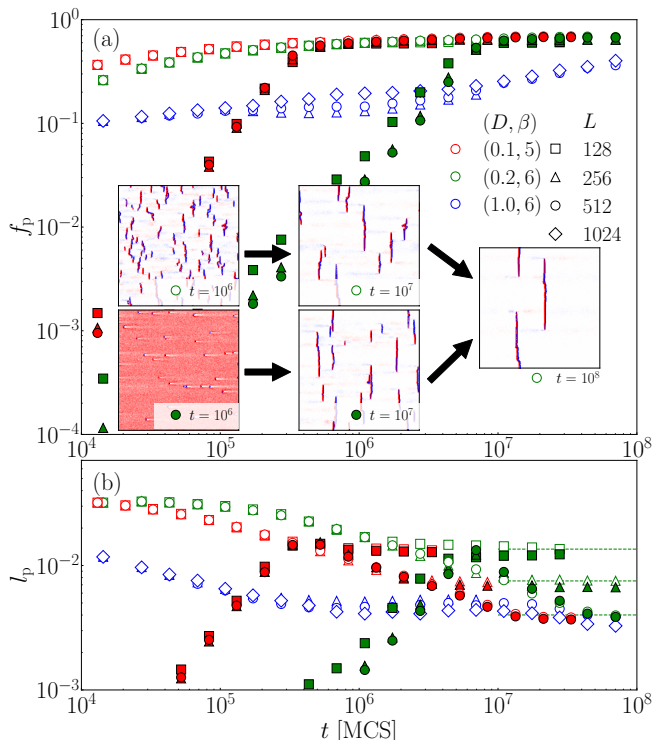


FIG. 2. f_p and l_p under a RIC (empty symbols) and an OIC (filled symbols) for a few values of (D, β) and $L_x = L_y = L$ as marked in Fig. 3(a) [Parameters: $\rho_0 = 4$ and $v = 1.0$]. Panels in (a) illustrate typical magnetization configurations, color-coded as in Fig. 1, in the transient, coarsening, and steady state regimes at $t = 10^6$, 10^7 , and 10^8 MCS, respectively, from both initial conditions when $L = 512$ and $(D, \beta) = (0.2, 6.0)$ [52]. The dashed lines in (b) indicate the scaling $l_p = O(L^{-1})$ at $(D, \beta) = (0.2, 6.0)$.

faces (PIs), and l_p , the total length of PIs per site. Under a random initial condition (RIC), PIs are created as randomly distributed domains collide with each other. The system undergoes a coarsening until reaching the state with $f_p = O(1)$ and $l_p = O(L_x^{-1})$ [55], wherein macroscopic PIs span the lattice in the y direction. This state will be referred to as a macroscopic PI state (MPIS). Under an ordered initial condition (OIC), the MPIS is accessible numerically for small values of D . In a short time regime, f_p increases super-linearly indicating that PIs are nucleated at a constant rate and their size grows. Then, the initial condition dependence disappears at a system-size-independent characteristic time and the system enters the coarsening regime to reach the MPIS. These results suggest that the MPIS constitutes a stable steady state phase.

A few remarks are in order. (i) Snapshots in Fig. 2 reveal a particle flux among PI segments. Individual resonating particles diffuse along a PI segment. Reaching an edge, they leak out and flow until being trapped in another segment. Due to this leak current, short PI segments blocked by longer ones shrink while longer ones

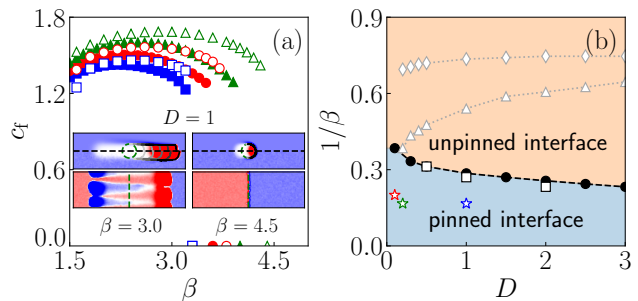


FIG. 3. (a) Propagation speed of a droplet from the MC simulations (empty symbols) and the hydrodynamic equation (filled symbols) [Parameters: $\rho_0 = 4$, $v = 1$, $D = 0.5$ (square), 1.0 (circle), and 2.0 (triangle)]. The insets depict a droplet at successive time steps from MC simulations (bottom half) and the hydrodynamic equation (top half). Snapshots of a spanning interface are also compared. (b) Phase diagram at $\rho_0 = 4$ and $v = 1$ with transition points marked with empty symbols (MC simulations) and filled symbols (hydrodynamic equation). The MIP transition line is compared with the metastable liquid-gas transition lines (dotted lines), which are estimated numerically from the binodal densities of metastable bands.

grow during the coarsening [52]. (ii) The system under the OIC could reach the MPIS within the simulation time scale only for small D . The relaxation dynamics is initiated by spontaneously nucleated and pinned droplets. Their nucleation time is known to increase exponentially with D [50]. We attribute the numerical difficulty to the rapid increase of the nucleation time. The coarsening dynamics becomes also slow as D increases. At $D = 1$, the systems with $L \gtrsim 1024$ have not reached the MPIS even at 10^8 MCS [52].

Interface dynamics is useful in investigating the MIP transition. Consider a spanning interface at $x = L_x/2$ separating the system into two halves. The interface roughens as domains penetrate into the other for $\beta < \beta_c$ while it is frozen for $\beta > \beta_c$ [52]. To pinpoint the transition point β_c , we introduce an isolated circular droplet into an ordered state and measure the speed c_f of the front [52]. As shown in Fig. 3(a), c_f from MC simulations and from numerical solutions of the space-discretized hydrodynamic equations (1) exhibits a discontinuous jump to zero at $\beta = \beta_c$. The resulting phase diagram is shown in Fig. 3(b). The speed and the phase diagram from both methods are in a qualitative agreement.

MIP from hydrodynamic theory – The hydrodynamic theory of Ref. [50] predicts a traveling droplet solution only. We revisit the hydrodynamic theory to reconcile it with the phenomenon of MIP. Consider a droplet of density ρ_d and magnetization $m_d = p\rho_d > 0$, whose front moves at a constant speed c_f on an ordered background characterized by particle density ρ_o and magnetization $m_o = -p\rho_o < 0$. The polarization $p > 0$ is determined

by $p = \tanh \beta p$. Mass conservation requires that $c_f = \frac{m_d + |m_o|}{m_d - |m_o|} pv = \frac{\rho_d + \rho_o}{\rho_d - \rho_o} pv$. Combined with a small density gradient expansion, the hydrodynamic equation leads to a simplified description for the magnetization $m(z)$ along the symmetry axis of a droplet [50, 56, 57]:

$$D_x \frac{d^2 m}{dz^2} = -\gamma(c_f) \frac{dm}{dz} - \frac{dV(m; c_f)}{dm}, \quad (2)$$

where $z = x - c_f t$ is the coordinate in the comoving frame, $\gamma(c_f) = c_f - v^2/c_f$, and $V(m; c_f) = \int F(\rho_o + v(m - m_o)/c_f, m) dm$ [see Ref. [50] for derivation]. Regarding m as a coordinate and z a time, this equation describes a damped motion of a particle of mass D_x under the inverted double-well potential $V(m; c_f)$ having two unstable fixed points at $m = m_o$ and m_d . The traveling droplet solution corresponds to the heteroclinic orbit connecting these two unstable fixed points. The condition that the excess potential energy $\Delta V := V(m_d; c_f) - V(m_o; c_f)$ is exactly dissipated by the damping term determines c_f self-consistently.

When β and c_f are large, the self-consistent equation admits an approximate solution. Due to mass conservation, we have $\Delta \rho := \rho_d - \rho_o = 2vp\rho_o/c_f + O(c_f^{-2})$ and $\Delta|m| := m_d - |m_o| = 2vp^2\rho_o/c_f + O(c_f^{-2})$. We can set the polarization $p = 1$ neglecting an $O(e^{-2\beta})$ correction. Keeping only the leading order term, we obtain

$$\Delta V = \int_{m_o}^{m_d} F dm = \frac{6v\rho_o^2}{\beta^2 c_f} e^\beta (1 + O(\beta^{-1}, c_f^{-1})). \quad (3)$$

The energy dissipation $E_d = \frac{1}{2} \int_{-\infty}^{\infty} \gamma |m'(z)|^2 dz$ is approximated as $E_d \simeq \gamma(m_d - m_o)^2 / \Delta z$, where Δz denotes a time required for a transition from m_d to m_o . For $m = m_o + \delta m$ with $|\delta m| \ll 1$, Eq. (2) becomes

$$D_x \delta m'' \simeq -\gamma \delta m' + k \delta m \quad (4)$$

with a stiffness constant $k = -\frac{dF}{dm}|_{m=m_o} \simeq e^\beta$, which yields that $\delta m \sim e^{-z/\tau_z}$ with

$$\tau_z = \frac{2D_x}{\gamma + \sqrt{\gamma^2 + 4D_x k}}. \quad (5)$$

Therefore, the transition time is given by $\Delta z = a\tau_z$ with a constant $a = O(1)$. Equating ΔV and E_d , we finally obtain

$$c_f \simeq \left(3av\sqrt{D_x}/2\right)^{1/2} \beta^{-1} e^{\beta/4}. \quad (6)$$

The exponential dependence in β is consistent with the numerical solution of Eq. (2) (not shown here).

The resulting density gradient $\Delta\rho/\Delta z \sim e^{\beta/4}$ grows exponentially with β , which makes the density gradient expansion worse and worse as β increases. We will argue that the traveling droplet solution breaks down beyond a threshold β_c using the resonance mechanism. We consider a simplified model consisting of only two sites A

and B , representing locations on the left and right of the droplet's front interface, respectively. During a time interval $\tau_f = e^{-\beta}$, $f_+ = \rho_d(D+v)\tau_f$ particles of positive spin flow from A to B , while $f_- = \rho_o(D+v)\tau_f$ particles of negative spin flow from B to A . We choose a specific value $\tau_f = e^{-\beta}$ so that spin flips are suppressed during this time interval. The droplet can move forward only if the invading particles (f_+) outnumber the remaining particles ($\rho_o - f_-$) at B . Otherwise, the invaders reverse their spin state and return back to site A , starting the resonating motion. Therefore, the traveling droplet solution requires $f_+ > \rho_o - f_-$, which imposes an upper bound for c_f :

$$c_f < v / (1 - 2(D+v)e^{-\beta}). \quad (7)$$

For large β , this bound decreases whereas the solution in Eq. (6) increases with β . This inconsistency implies the existence of a threshold value β_c , beyond which the resonance sets in and interfaces become pinned.

Coarsening dynamics of pinned interfaces – To shed a light on the coarsening dynamics of PIs, we develop a theory governing the time evolution of the length of PI segments. It is analytically tractable when $D/v \ll 1$ and $\beta \gg 1$. We will keep only the leading order term neglecting $O(l^{-1}, D/v, e^{-\beta})$ corrections in this section.

Consider a PI segment of length l in a homogeneous background of $+$ spins. Particles of total flux $F = \rho_o vl$ land on the PI, jump across it at rate $D+v$, diffuse along it at rate D , and leak away at both end. Assuming that $D/v \ll 1$, we model the PI segment as two unit-width columns of $+$ spins and $-$ spins with the leak current channels of unit width at both ends. Let P (M) be the terminal site of the positive (negative) domain, in one end, and P' (M') be the neighboring site through which leaking $+$ particles flow. Flux balance conditions yield that the mean occupation numbers at those sites are given by $N_P \simeq N_M \simeq \rho_o vl / (4D)$, $N_{P'} \simeq \rho_o l / 4$, and $N_{M'} \simeq \rho_o l / 2$.

The PI segment can *grow* by one lattice unit for a time interval τ_f if $-$ particles hopping from M outnumber $+$ particles residing at M' . For large l , the number of hopping particles n follows a Gaussian distribution of mean $\langle n \rangle = N_M D \tau_f$ and variance $\sigma_n^2 = N_M D \tau_f (1 - D \tau_f)$. Thus, the growth probability is given by $P_g \simeq \frac{1}{\sqrt{2\pi}} \int_{z_g}^{\infty} e^{-z^2/2} dz \simeq \frac{1}{\sqrt{2\pi z_g^2}} e^{-z_g^2/2}$ with $z_g := (N_{M'} - \langle n \rangle) / \sqrt{\sigma_n^2} \simeq \sqrt{\frac{\rho_o l}{v \tau_f}}$. On the other hand, it can *shrink* by one lattice unit if $+$ particles jumping from P outnumber $-$ particles at M . Using the similar Gaussian statistics, we find that the shrink probability is given by $P_s \simeq \frac{1}{\sqrt{2\pi}} \int_{z_s}^{\infty} e^{-z^2/2} dz$ with $z_s \simeq \sqrt{\frac{\rho_o l}{4D \tau_f}}$. Thus, the rate $W = P/\tau_f$ follows the exponential scaling law

$$W(l) \sim e^{-l/l_0} \quad (8)$$

for large l , where $l_0 = l_g \simeq 2v\tau_f/\rho_0$ for growth and $l_0 = l_s \simeq 8D\tau_f/\rho_0$ for shrink. The growth is dominant ($l_g > l_s$) for small D/v region, which explains the emergence of the MPIS observed in Fig. 2. The exponential scaling law and the dominance of the growth ($l_g > l_s$) have been confirmed numerically for $D/v \leq 1.0$ at $\beta = 5$ [52].

Discussions – We have discovered a novel phenomenon of MIP in the AIM. Pinning typically occurs due to defects or impurities [34, 37, 58–60]. Our work reveals a unique mechanism for pinning in the absence of quenched disorder: a resonating back-and-forth motion of SPPs. We have also studied the active p -state clock model, in which the self-propulsion direction is modeled with p -state clock spins. We observed the MIP phenomenon for $p \leq 4$ [52], which will be presented elsewhere.

Contrary to early expectations [24, 25, 48], the AIM does not exhibit the liquid-gas transition due to the droplet excitation [50]. Instead, it displays the MIP transition. The nature of the asymptotic steady state below the MIP transition is determined by the growth and shrink dynamics of PIs. Our numerical and analytic results have shown that the growth is dominant and the system relaxes to the MPIS for small D/v region. On the other hand, the spontaneous nucleation of droplets [50] and the coarsening dynamics of PIs become extremely slow as D increases, which hinders probing the nature of the steady state in the whole region below the pinning transition. Since the competition between growth and shrink can have a profound impact on the global polar order, it calls for further studies especially in the large D/v region, which is left for future work.

We acknowledge fruitful discussions with Heiko Rieger, Sunghan Ro, and Yarif Kafri. This work is supported by the National Research Foundation of Korea (NRF) grant funded by the Korea government (MSIT) (No. RS-2024-00348526). We also acknowledge the computing resources of Urban Big data and AI Institute (UBAI) at the University of Seoul.

-
- [1] M. C. Marchetti, J.-F. Joanny, S. Ramaswamy, T. B. Liverpool, J. Prost, M. Rao, and R. A. Simha, Hydrodynamics of soft active matter, *Reviews of Modern Physics* **85**, 1143 (2013).
 - [2] C. Bechinger, R. Di Leonardo, H. Löwen, C. Reichhardt, G. Volpe, and G. Volpe, Active particles in complex and crowded environments, *Reviews of Modern Physics* **88**, 045006 (2016).
 - [3] R. Di Leonardo, L. Angelani, D. Dell’Arciprete, G. Ruocco, V. Iebba, S. Schippa, M. P. Conte, F. Mecarini, F. De Angelis, and E. Di Fabrizio, Bacterial ratchet motors, *Proceedings of the National Academy of Sciences* **107**, 9541 (2010).
 - [4] L. Huber, R. Suzuki, T. Krüger, E. Frey, and A. Bausch, Emergence of coexisting ordered states in active matter systems, *Science* **361**, 255 (2018).
 - [5] S. Henkes, K. Kostanjevec, J. M. Collinson, R. Sknepnek, and E. Bertin, Dense active matter model of motion patterns in confluent cell monolayers, *Nature Communications* **11**, 1405 (2020).
 - [6] J. Buhl, D. J. Sumpter, I. D. Couzin, J. J. Hale, E. Despland, E. R. Miller, and S. J. Simpson, From disorder to order in marching locusts, *Science* **312**, 1402 (2006).
 - [7] I. Giardina, Collective behavior in animal groups: theoretical models and empirical studies, *HFSP Journal* **2**, 205 (2008).
 - [8] M. Ballerini, N. Cabibbo, R. Candelier, A. Cavagna, E. Cisbani, I. Giardina, V. Lecomte, A. Orlandi, G. Parisi, A. Procaccini, *et al.*, Interaction ruling animal collective behavior depends on topological rather than metric distance: Evidence from a field study, *Proceedings of the national academy of sciences* **105**, 1232 (2008).
 - [9] A. J. Ward, D. J. Sumpter, I. D. Couzin, P. J. Hart, and J. Krause, Quorum decision-making facilitates information transfer in fish shoals, *Proceedings of the National Academy of Sciences* **105**, 6948 (2008).
 - [10] A. Cavagna and I. Giardina, Bird flocks as condensed matter, *Annu. Rev. Condens. Matter Phys.* **5**, 183 (2014).
 - [11] A. Cavagna, D. Conti, C. Creato, L. Del Castello, I. Giardina, T. S. Grigera, S. Melillo, L. Parisi, and M. Viale, Dynamic scaling in natural swarms, *Nature Physics* **13**, 914 (2017).
 - [12] A. Bricard, J.-B. Caussin, N. Desreumaux, O. Dauchot, and D. Bartolo, Emergence of macroscopic directed motion in populations of motile colloids, *Nature* **503**, 95 (2013).
 - [13] N. Kumar, H. Soni, S. Ramaswamy, and A. Sood, Flocking at a distance in active granular matter, *Nature communications* **5**, 4688 (2014).
 - [14] J. Yan, M. Han, J. Zhang, C. Xu, E. Luijten, and S. Granick, Reconfiguring active particles by electrostatic imbalance, *Nature Materials* **15**, 1095 (2016).
 - [15] B. Liebchen and H. Lowen, Synthetic chemotaxis and collective behavior in active matter, *Accounts of Chemical Research* **51**, 2982 (2018).
 - [16] T. Vicsek, A. Czirók, E. Ben-Jacob, I. Cohen, and O. Shochet, Novel type of phase transition in a system of self-driven particles, *Physical Review Letters* **75**, 1226 (1995).
 - [17] J. Toner and Y. Tu, Long-range order in a two-dimensional dynamical xy model: how birds fly together, *Physical Review Letters* **75**, 4326 (1995).
 - [18] N. D. Mermin and H. Wagner, Absence of ferromagnetism or antiferromagnetism in one-or two-dimensional isotropic heisenberg models, *Physical Review Letters* **17**, 1133 (1966).
 - [19] Y. Fily and M. C. Marchetti, Athermal phase separation of self-propelled particles with no alignment, *Physical Review Letters* **108**, 235702 (2012).
 - [20] I. Buttinoni, J. Bialké, F. Kümmel, H. Löwen, C. Bechinger, and T. Speck, Dynamical clustering and phase separation in suspensions of self-propelled colloidal particles, *Physical Review Letters* **110**, 238301 (2013).
 - [21] M. E. Cates and J. Tailleur, Motility-induced phase separation, *Annu. Rev. Condens. Matter Phys.* **6**, 219 (2015).
 - [22] L. Caprini, U. M. B. Marconi, and A. Puglisi, Spontaneous Velocity Alignment in Motility-Induced Phase Separation, *Physical Review Letters* **124**, 078001 (2020).
 - [23] Z. Csahók and T. Vicsek, Lattice-gas model for collective biological motion, *Physical Review E* **52**, 5297 (1995).

- [24] A. P. Solon and J. Tailleur, Revisiting the flocking transition using active spins, *Physical Review Letters* **111**, 078101 (2013).
- [25] A. P. Solon and J. Tailleur, Flocking with discrete symmetry: The two-dimensional active ising model, *Physical Review E* **92**, 042119 (2015).
- [26] M. Mangeat, S. Chatterjee, R. Paul, and H. Rieger, Flocking with a q-fold discrete symmetry: Band-to-lane transition in the active potts model, *Physical Review E* **102**, 042601 (2020).
- [27] S. Chatterjee, M. Mangeat, R. Paul, and H. Rieger, Flocking and reorientation transition in the 4-state active potts model, *Europhysics Letters* **130**, 66001 (2020).
- [28] F. Dittrich, T. Speck, and P. Virnau, Critical behavior in active lattice models of motility-induced phase separation, *The European Physical Journal E* **44**, 1 (2021).
- [29] A. Solon, H. Chaté, J. Toner, and J. Tailleur, Susceptibility of polar flocks to spatial anisotropy, *Physical Review Letters* **128**, 208004 (2022).
- [30] S. Chatterjee, M. Mangeat, and H. Rieger, Polar flocks with discretized directions: the active clock model approaching the vicsek model, *Europhysics Letters* **138**, 41001 (2022).
- [31] A. M. Menzel, Collective motion of binary self-propelled particle mixtures, *Physical Review E* **85**, 021912 (2012).
- [32] M. Fruchart, R. Hanai, P. B. Littlewood, and V. Vitelli, Non-reciprocal phase transitions, *Nature* **592**, 363 (2021).
- [33] S. Chatterjee, M. Mangeat, C.-U. Woo, H. Rieger, and J. D. Noh, Flocking of two unfriendly species: The two-species vicsek model, *Physical Review E* **107**, 024607 (2023).
- [34] O. Chepizhko and F. Peruani, Diffusion, Subdiffusion, and Trapping of Active Particles in Heterogeneous Media, *Physical Review Letters* **111**, 160604 (2013).
- [35] S. Ro, Y. Kafri, M. Kardar, and J. Tailleur, Disorder-Induced Long-Ranged Correlations in Scalar Active Matter, *Physical Review Letters* **126**, 048003 (2021).
- [36] Y. Duan, B. Mahault, Y.-q. Ma, X.-q. Shi, and H. Chaté, Breakdown of ergodicity and self-averaging in polar flocks with quenched disorder, *Physical Review Letters* **126**, 178001 (2021).
- [37] D. Vahabli and T. Vicsek, Emergence of synchronised rotations in dense active matter with disorder, *Communications Physics* **6**, 56 (2023).
- [38] J. Toner and Y. Tu, Flocks, herds, and schools: A quantitative theory of flocking, *Physical Review E* **58**, 4828 (1998).
- [39] G. Grégoire and H. Chaté, Onset of collective and cohesive motion, *Physical Review Letters* **92**, 025702 (2004).
- [40] E. Bertin, M. Droz, and G. Grégoire, Boltzmann and hydrodynamic description for self-propelled particles, *Physical Review E* **74**, 022101 (2006).
- [41] H. Chaté, F. Ginelli, G. Grégoire, and F. Raynaud, Collective motion of self-propelled particles interacting without cohesion, *Physical Review E* **77**, 046113 (2008).
- [42] H. Chaté, F. Ginelli, G. Grégoire, F. Peruani, and F. Raynaud, Modeling collective motion: variations on the vicsek model, *The European Physical Journal B* **64**, 451 (2008).
- [43] E. Bertin, M. Droz, and G. Grégoire, Hydrodynamic equations for self-propelled particles: microscopic derivation and stability analysis, *Journal of Physics A: Mathematical and Theoretical* **42**, 445001 (2009).
- [44] G. Baglietto and E. V. Albano, Nature of the order-disorder transition in the vicsek model for the collective motion of self-propelled particles, *Physical Review E* **80**, 050103 (2009).
- [45] T. Ihle, Invasion-wave-induced first-order phase transition in systems of active particles, *Physical Review E* **88**, 040303 (2013).
- [46] M. Kourbane-Houssene, C. Erignoux, T. Bodineau, and J. Tailleur, Exact Hydrodynamic Description of Active Lattice Gases, *Physical Review Letters* **120**, 268003 (2018).
- [47] M. Scandolo, J. Pausch, and M. E. Cates, Active Ising Models of flocking: a field-theoretic approach, *The European Physical Journal E* **46**, 103 (2023).
- [48] A. P. Solon, H. Chaté, and J. Tailleur, From phase to microphase separation in flocking models: The essential role of nonequilibrium fluctuations, *Physical Review Letters* **114**, 068101 (2015).
- [49] J. Codina, B. Mahault, H. Chaté, J. Dobnikar, I. Pagonabarraga, and X.-q. Shi, Small obstacle in a large polar flock, *Physical Review Letters* **128**, 218001 (2022).
- [50] B. Benvegnen, O. Granek, S. Ro, R. Yaacoby, H. Chaté, Y. Kafri, D. Mukamel, A. Solon, and J. Tailleur, Metastability of Discrete-Symmetry Flocks, *Physical Review Letters* **131**, 218301 (2023).
- [51] We confirmed that the results are qualitatively the same under the parallel update and the random sequential update.
- [52] See Supplemental Material.
- [53] P. Muller, Glossary of terms used in physical organic chemistry (IUPAC Recommendations 1994), *Pure and Applied Chemistry* **66**, 1077 (1994).
- [54] B. Benvegnen, H. Chaté, P. L. Krapivsky, J. Tailleur, and A. Solon, Flocking in one dimension: Asters and reversals, *Physical Review E* **106**, 054608 (2022).
- [55] The finite size scaling behavior $l_p = O(L_x^{-1})$ has been confirmed in rectangular systems with $L_x \neq L_y$.
- [56] J.-B. Caussin, A. Solon, A. Peshkov, H. Chaté, T. Dauxois, J. Tailleur, V. Vitelli, and D. Bartolo, Emergent Spatial Structures in Flocking Models: A Dynamical System Insight, *Physical Review Letters* **112**, 148102 (2014).
- [57] A. P. Solon, J.-B. Caussin, D. Bartolo, H. Chaté, and J. Tailleur, Pattern formation in flocking models: A hydrodynamic description, *Physical Review E* **92**, 062111 (2015).
- [58] F. Peruani and I. S. Aranson, Cold Active Motion: How Time-Independent Disorder Affects the Motion of Self-Propelled Agents, *Physical Review Letters* **120**, 238101 (2018).
- [59] P. Forgács, A. Libál, C. Reichhardt, and C. J. O. Reichhardt, Active matter shepherding and clustering in inhomogeneous environments, *Physical Review E* **104**, 044613 (2021).
- [60] G. K. Sar, D. Ghosh, and K. O’Keeffe, Pinning in a system of swarmalators, *Physical Review E* **107**, 024215 (2023).

Supplemental Materials for “Motility-Induced Pinning in Flocking System with Discrete Symmetry”

Chul-Ung Woo and Jae Dong Noh

Department of Physics, University of Seoul, Seoul 02504, Korea

Appendix A: Supplementary animations

- File `1_droplets_OIC.mp4` corresponds to the supplementary movie for Fig. 1. It shows a time evolution of the microscopic model from a homogeneous ordered state to a state with nucleated droplets. Parameters: $L_x = L_y = 4096, \rho_0 = 8, \beta = 2, v = 1, D = 0.05$.
- File `2_droplets_band.mp4` corresponds to the supplementary movie showing a time evolution of the microscopic model from a macrophase separated state to a state with nucleated droplets. Parameters: $L_x = 2048, L_y = 256, \rho_0 = 3, \beta = 2, v = 1, D = 0.1$.
- Files `3_MIP_RIC.mp4` and `4_MIP_OIC.mp4` correspond to the supplementary movies for the insets of Fig. 2(a). These videos demonstrate the time evolution from the random initial condition and ordered initial condition, respectively, into the motility-induced pinning phase in the microscopic model. Parameters: $L_x = L_y = 512, v = 1, D = 0.2, \beta = 6, \rho_0 = 4$.
- File `5_MIP_RIC_largeL.mp4` corresponds to the supplementary movie for Fig. 2. It demonstrates a slow relaxation dynamics to the motility-induced pinning phase in the microscopic model. Parameters: $L_x = L_y = 4096, v = 1, D = 1, \beta = 5, \rho_0 = 4$.
- Files `6_droplet.mp4` and `7_droplet_DHE.mp4` are the supplementary movies for the insets of Fig. 3 (a). They show the time evolution of an isolated circular droplet of radius $r_0 = 50$ in the ordered background in the microscopic model and the discretized hydrodynamic equation, respectively. Parameters: $L_x = 1024, L_y = 256, v = 1, D = 1, \rho_o = 4$.
- File `8_ACM_droplet.mp4` is the supplementary movie for the last paragraph of the main text. It shows the motion of pinned and unpinned droplets in the active p -state clock model with $p = 4$ (left column) and $p = 8$ (right column) in the microscopic model (top row) and in the discretized hydrodynamic equation (bottom row). Parameters: $L_x = L_y = 1024, \rho_o = 10, \beta = 6, v = 1, D = 1$.

Appendix B: Growth and shrink rates of a pinned interface

We examined numerically the exponential scaling law $W_{g,s}(l) \sim e^{-l/l_{g,s}}$ for the growth and shrink rates of a PI derived in the main text. When $\beta > \beta_c$, the rates were measured in the following way:

1. The system is prepared to be in an ordered state with a PI of length l being implanted. Namely, all lattice sites are occupied by $+$ particles of mean density ρ_0 except for those within a $(2 \times l)$ rectangle. They are occupied by ρ'_0 ($> \rho_0$) particles whose spin states are $+$ in the $(1 \times l)$ column on the left and $-$ in the $(1 \times l)$ column on the right.
2. A PI is identified as an interface between positively and negatively polarized domains. The occupation numbers at sites along the domain boundary are required to be larger than a cutoff value $\rho_{\text{cutoff}} = 5\rho_0$.
3. During simulations up to 10^7 MCS, we record the time trajectory $\{l_n = l(t = t_n)\}$ of the PI length at discrete time steps $t_n = n\tau_0$ with $n \in \mathbb{Z}$ and $\tau_0 = 10^3$. To reduce an artifact from short-time fluctuations, l_n represents a running average over the time interval $t_{n-n_0} < t < t_n$ with $n_0 = 10$.
4. Given a trajectory $\{l_n\}$, we count $N_{l \rightarrow l \pm 1}$, the number of jumps in l_n from l to $l \pm 1$, and T_l , the total time span in which $l_n = l$. The growth rate $W_g(l)$ and the shrink rate $W_s(l)$, per unit MCS, are given by $N_{l \rightarrow l+1}/T_l$ and $N_{l \rightarrow l-1}/T_l$, respectively, which are then averaged over more than 10^3 independent trajectories.

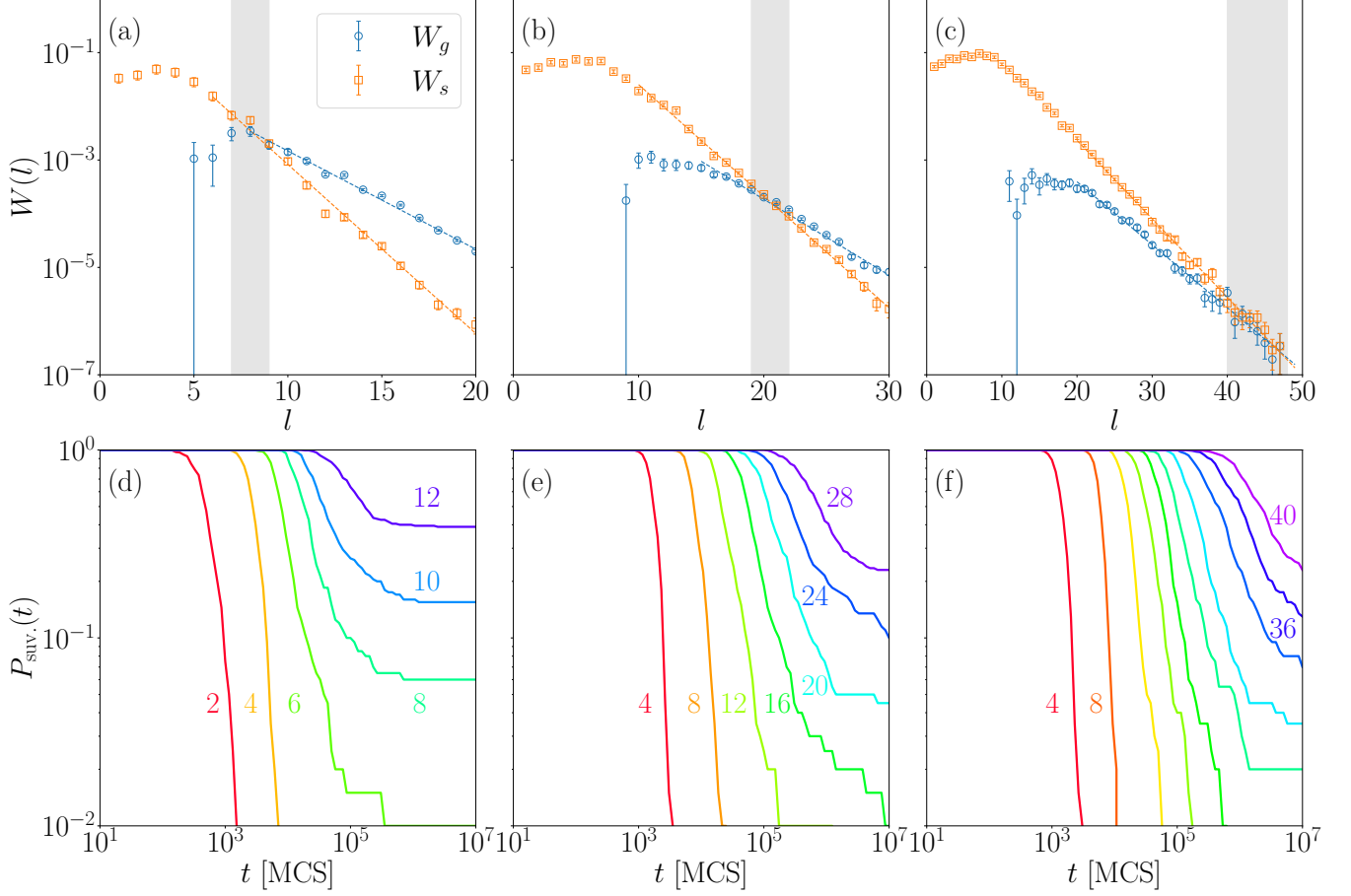


FIG. S1. Growth (W_g) and shrink (W_s) rates per unit MCS of an isolated PI of size l for $D = 0.5$ in (a), 0.8 in (b), and 1.0 in (c). The shaded vertical bars represent the threshold value l_{th} , beyond which the growth is dominant. Survival probability $P_{suv.}(t)$ of an isolated PI imposed by a droplet of diameter l for $D = 0.5$ in (d), $D = 0.8$ in (e), and $D = 1.0$ in (f). [Parameters: $L_x = 1024$, $L_y = 128$, $v = 1$, $\beta = 5$, $\rho_0 = 4$, $\rho'_0 = 200$]

The growth and shrink rates are presented in Fig. S1 (a-c). The numerical data clearly demonstrate the exponential scaling law and that $l_g > l_s$ for the parameter values considered. We also notice the existence of a threshold size l_{th} : shorter PIs with $l < l_{th}$ tend to evaporate while longer PIs with $l > l_{th}$ tend to grow. It is analogous to the critical nucleation size in the equilibrium nucleation theory for supersaturated gas systems. The threshold value increases as D increases: $l_{th.} \simeq 8.0$ at $D = 0.5$, $\simeq 20.0$ at $D = 0.8$, and $\simeq 45.0$ at $D = 1.0$. It explains the reason why the system starting from OIC takes longer time to relax to the MPIS.

An isolated PI with $l \ll l_{th.}$ shrinks and evaporates eventually. We confirmed this phenomenon by measuring the survival probability $P_{suv.}(t)$ of an isolated PI generated from a circular droplet of diameter l embedded in a homogeneous ordered state of density ρ_0 (see Fig. 3 of the main text). The initial particle density of the droplet is taken to be $5\rho_0$. The survival probability is given by the fraction of samples with a surviving PI among all independent 200 samples. Figure S1 (d-f) presents the plots of $P_{suv.}(t)$ in the log-log scale. For small l , the long time tail of $P_{suv.}(t)$ is characterized by a downward curvature. However, the tail becomes flatter as l increases, and attains an upward curvature for large l . The crossover occurs around the threshold size $l_{th.}$. Thus, we expect that the PI larger than the threshold size has a finite survival probability.